NOAA Technical Memorandum ERL WMPO-46

ON THE DETERMINATION OF PRECIPITATION EFFICIENCY

Herbert Riehl
Gary Williams

Weather Modification Program Office
Boulder, Colorado
November 1981

noaa NATIONAL OCEANIC AND ATMOSPHERIC ADMINISTRATION / Environmental Research Laboratories

NOAA Technical Memorandum ERL WMPO-46

ON THE DETERMINATION OF PRECIPITATION EFFICIENCY

Herbert Riehl
Gary Williams

Weather Modification Program Office
Boulder, Colorado
November 1981

UNITED STATES
DEPARTMENT OF COMMERCE

Malcolm Baldrige,
Secretary

NATIONAL OCEANIC AND
ATMOSPHERIC ADMINISTRATION

John V. Byrne,
Administrator

Environmental Research
Laboratories

George H. Ludwig
Director

NOTICE

Mention of a commercial company or product does not constitute an endorsement by NOAA Environmental Research Laboratories. Use for publicity or advertising purposes of information from this publication concerning proprietary products or the tests of such products is not authorized.

CONTENTS

ON THE DETERMINATION OF PRECIPITATION EFFICIENCY

Herbert Riehl[1] and Gary Williams

ABSTRACT. Assuming conservation of energy, an air column may be followed across an obstacle such as a mountain range, and also a convergence zone. The efficiency of this zone for releasing water or ice toward the ground may be computed from the ratio of the difference in specific humidity at the inflow and outflow end of the computation boundary to the difference in specific humidity at the inflow and at the greatest height, or lowest pressure, attained by the column. This method was applied to storms crossing the Wasatch Mountains of southern Utah for January to March 1981. Efficiency near 100 percent was determined for more than half of the sample of 18 cases. Further, nearly 60 percent of the imported moisture was left over the mountains in these efficient cases, a high value. The two controls of the total precipitate, moisture difference between inflow and outflow, and strength of total mass flow, contributed equally to the fallout. Synoptically, most situations involved short wave troughs in the westerlies, as was expected. In post-experiment analysis, it was found that most of the trajectories followed across the mountain area were on the cyclonic shear side of jet streams; this was not anticipated. The computational technique is illustrated with two examples, one with northwest and the other with southwest upper flow.

1. Introduction--Definitions of Efficiency

In the frequently occurring situations when there is a vast amount of interaction between a number of individual clouds and the space between them, a measure of the efficiency of the aggregate in delivering moisture to the ground can be obtained. One frequently proposed technique consists of looking at the cloud conglomeration as a whole from its boundary. Efficiency is defined as precipitation/moisture inflow. In winter situations over land this measure is readily determined from line integral calculations of moisture import through a fixed boundary with a precipitation gage network inside. A difficulty is that much if not most of the water vapor passing through the system never reaches condensation; i.e., there are no changes in phase which are really the main objective of efficiency calculation and use. Especially in stratus clouds, which are elongated and flat, the difference in saturation vapor pressure or saturation specific humidity (q_s) between top and bottom will be small. In strong wind conditions a huge vapor flux in and out will result, leading to a gross underestimate of the in-cloud physical cycle which is of primary importance.

This problem will be avoided if efficiency (E) is computed only with respect to the moisture that actually condenses in a given system, the condensate (C). Here the fluxes of water vapor never reaching the condensation stage are excluded. One can write that

---

[1]Cooperative Institute for Research in the Environmental Sciences, Boulder, Colo.

$$C = Pr + W, \qquad (1)$$

where Pr is the "precipitate", the total mass of ice or water falling out (units mass/time), and W will stand here for the rain or snow evaporation within the atmosphere. W will be very small where cloud bases are low and the ambient atmosphere is near saturation. In contrast, in areas with high cloud bases and clouds protruding into an environment with, perhaps, 50 percent relative humidity, W is likely to be large, especially when it is considered that, in the presence of substantial vertical shear of the horizontal wind, the falling water may pass through a thickness of several kilometers of outside air, leaving nothing but virga.

An appropriate measure of efficiency lending prominence to such variable atmospheric structures is

$$E = Pr/C \quad . \qquad (2)$$

Our main concern will be with this measure. It may be noted that Pr is related to the precipitation (P) with units mass/area/time through the precipitation rate which is Pr/A (A = area). Precipitation is then obtained by assigning a duration to the precipitation rate. These two factors, variable area of deposition and duration, are really extraneous to the efficiency problem, since they depend on such things as size and propagation rate of a synoptic system and the angle at which it may happen to cross a given region. With these considerations eq. (2) appears to be a particularly desirable form for computation.

The ratio E = Pr/C cannot be obtained from line integrals giving net moisture convergence, since the evaporative effect is already included in this computation. Hence computation is not very easy. Following considerations from tropical meteorology a practical method was proposed by Rasmussen et al. (1969) using a Midwest cyclone as an example. This method uses the principle of conservation of energy; "tubes" of constant energy are followed through a precipitation area, essentially a LaGrangian technique. For periods of 12-24 hours, only changes of sensible and latent heat need to be considered; kinetic energy usually is negligible, and allowance can be made readily for radiation heat losses. For nearly all purposes the well-known form of the first law of thermodynamics can be expected to hold, namely,

$$- L\, dq = c_p T/\theta \, d\theta \quad , \qquad (3)$$

where L is latent heat of condensation, c_p specific heat at constant pressure, T temperature of condensation, and θ potential temperature. In cold winter storm cases we may prefer to use Sdq = (L + F) dq, where S is heat of sublimation, virtually a constant, and F is latent heat of fusion. On account of the fraction T/θ, eq. (3) is difficult to evaluate; however, the level of reference (θ_o) is arbitrary. For the case of airflow over mountains with average top near 700 mb here to be analyzed, the 700 mb level may be taken for θ_o instead of the common 1000 mb; there $\theta_o = T$. When flow is considered to ascend on the windward and descend on the leeward side of mountains, the error in setting $T/\theta = 1$ is well within range of the accuracy of the observations. With this approximation eq. (3) may be integrated, and

$$cp\theta + Sq = \text{const} = Q \quad , \qquad (4)$$

the energy in the tube to be followed.

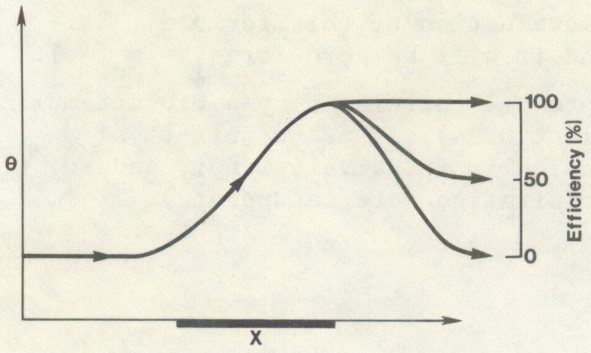

Figure 1.--Variation of potential temperature in an energy tube during passage over a mountain range (represented by heavy line at the bottom).

Figure 1 shows the variation, in an energy tube, of potential temperature during passage through a convergence zone or movement over a mountain range. Relative humidity of 100 percent is reached somewhere near the start of the zone of ascent; sublimation ends at the downstream end of this zone where, from eq. (4), θ attains its highest value, because the entire condensation process will be completed at this point.

If all condensation product falls out as precipitate (Pr), the efficiency of the moist process is given by E = Pr/C = 100 percent. If all condensed material reevaporates in the air, E = 0. All other values are intermediate. Cirrus traveling long distances from the condensation area will not be considered here.

The problem is that of modeling the atmosphere in the energy tube at the top of ascent, hereafter called "mountain sonde" for the purpose of this report. The modeling method will be discussed later; for the present we shall assume that $\hat{\theta}$ and $\hat{q}$ at the peak are known; the caret denotes averages over the pressure depth of the tube. The mass flow of air (M) in the tube must be a constant since, from continuity, as much mass must come out as goes in, ignoring any potential thickening or thinning of the tube as a small effect. Then, with conservation of energy included, $\hat{M}\hat{Q}$ = constant along the whole path of the energy tube. Since $\hat{Q}$ is a constant in the tube, $\hat{M}\hat{Q} = \hat{M}\,\hat{Q}$ or

$$\hat{M}\,\hat{Q} = \hat{M}\,(c_p\hat{\theta} + S\hat{q}) = \text{constant} \quad . \tag{5}$$

With the subscripts "i" for inflow, "mtn" for mountain and "o" for outflow,

$$\hat{M}\,(c_p\hat{\theta}_i + S\hat{q}_i) = \hat{M}\,(c_p\hat{\theta}_{mtn} = S\hat{q}_{mtn}) = \hat{M}\,(c_p\hat{\theta}_o + S\hat{q}_o) \quad . \tag{6}$$

It follows that the condensate $C \propto \hat{q}_i - \hat{q}_{mtn}$ and that $Pr \propto \hat{q}_i - \hat{q}_o$. Then the definition of efficiency for an energy tube becomes

$$E = Pr/C = (\hat{q}_i - \hat{q}_o)/(\hat{q}_i - \hat{q}_{mtn}) \quad . \tag{7}$$

A main purpose of this paper will be the evaluation of this formula. Evidently, E = 100 percent for $\hat{q}_o = \hat{q}_{mtn}$, and it will be zero for $\hat{q}_i = \hat{q}_o$. It may be noted that Pr and precipitation rate are correlated by a product-moment coefficient of 0.83 (tetrachoric coefficient 0.94). Thus the effect of variation of the area receiving precipitation is relatively minor, and eq. (7) often may be closely interpreted as (precipitation rate/condensate).

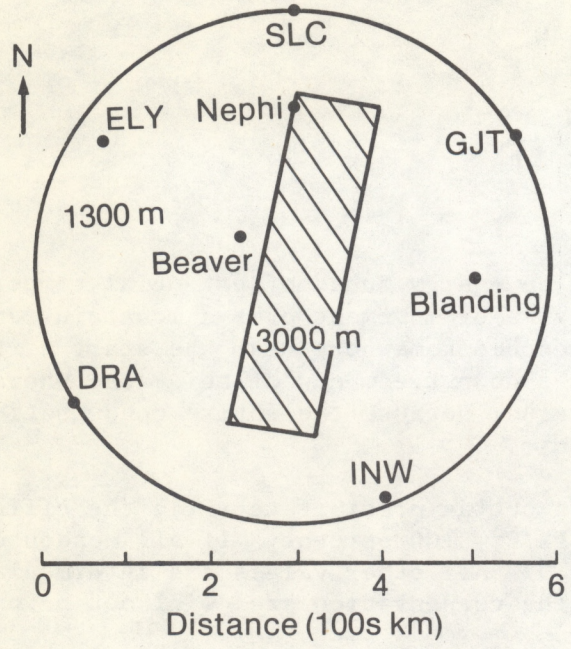

Figure 2.--Wasatch area and stations used for computations. Mean elevations of windward plain and mountain top area are indicated.

2. Area and Observations

The occasion for making the calculations described in this report is the winter cloud-seeding program carried out in the southern Wasatch mountains of Utah beginning in 1974. A large evaluation program was carried out in the 1980-81 season; the present independent research was timed to coincide with the evaluation period. It so happened that the winter was completely dry until late January 1981, followed by intermittent synoptic weather systems through February and March. Thus the period of calculations covered most precipitation received during the entire winter.

Figure 2 shows the mountain range in simplified form, the mean height of the mountains and of the approach plains to the west, the closest ring of rawinsonde stations, and the location of three rawinsonde stations maintained intermittently by the State of Utah. The symbols denote stations of the National Weather Service:

SLC Salt Lake City, Utah
ELY Ely, Nev.
DRA Desert Rock (Las Vegas), Nev.
INW Winslow, Ariz.
GJT Grand Junction, Colo.

Our work is based mainly on these five stations; observations of the special stations were used whenever possible. Almost all cases of the 1980-81 season as well as of previous seasons were seeded; this should be kept in mind when reading the subsequent parts of this report. Because of the prime reliance on the five rawinsonde stations the computations can be extended to previous years and to a long series of years before seeding began. According to Hill (1977) the most suitable pre-seeding period consists of the seven winters 1966-73, which followed a change in the NOAA rawinsonde moisture element. Therefore a large sample of cases can be gathered retroactively to evaluate eq. (7) and Figure 1. We made computations for 22 cases, most of them 12-hour periods corresponding the the most frequent time interval for crossing of air from windward to leeward stations. Of these cases, two barely reached condensation and were discarded; in one the winds transported the air across the mountains in 6 hours, and on three occasions a closed low was stationary in the middle of the circle without an organized trans-mountain flow. Thus 16 cases remained for close examination. On additional occasions the flow was strongly from the south and did not cross the mountains; these could not be considered at all. Of the 16 cases, about 10 proved fairly simple and 6 more difficult. An average season, not so dry as the one analyzed, should have easily 10-20 simple cases. Even if only these are included in historical calculations, a large sample of seeded and unseeded cases is available for comparison.

In view of the prevailing winds and tracks of synoptic systems, ELY and DRA were the stations mainly giving inflow data, GJT outflow data; SLC and INW were used more rarely. But depending on the winds, combinations SLC-ELY and ELY-DRA were also used to determine inflow parameters with linear interpolation between stations; SLC-GJT and GJT-INW similarly served for the outflow.

The principal steps of the computation technique will be described later with two individual cases; general results in terms of statistics and the synoptic background will be presented first.

3. Statistical Results

3.1 Frequencies

Efficiency above 80 percent predominates (Fig. 3) with 12 values out of 18, which number includes the two cases with zero efficiency (no ascent beyond the condensation level). Grand Junction sondes on the outflow sides are normally very dry compared with the windward side, a typical picture for mountain ranges. We presume that the fallout of moisture occurs over the mountains where cloud base in most cases is on the mountain or slightly above it, so that there will be no evaporation over the range itself. Snow or rain falling out beyond the range can evaporate below the energy tube; Grand Junction is far away. This is a possibility that could not be measured; one would need two stations close to the mountains on the lee side. With such stations the possible range of calculations would be greatly extended.

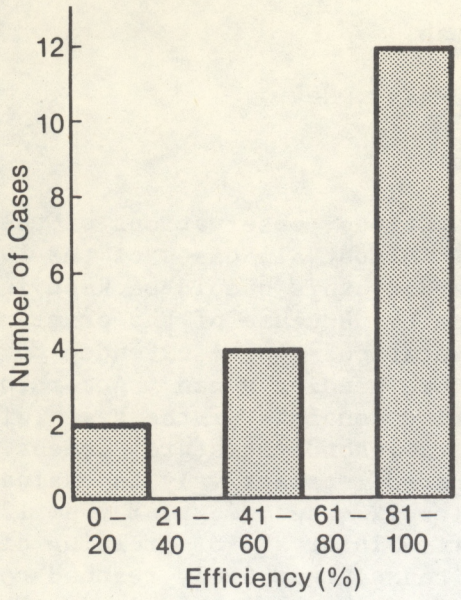

Figure 3.--Frequency distribution of class intervals of efficiency determined from equation 7.

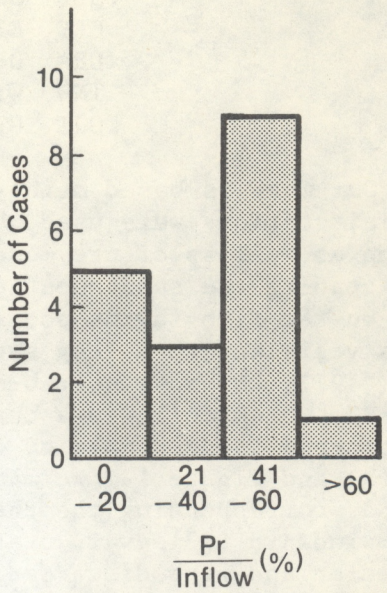

Figure 4.--Frequency distribution of class intervals of precipitate/inflow.

Efficiency measured as precipitate/moisture-inflow can also be determined from the energy tube; usually, one can approximate $Pr = \hat{M} (\hat{q}_i - \hat{q}_o)$ and the moisture inflow by $M_i = \hat{M} \hat{q}_i$. This measure of efficiency so computed has a pronounced maximum frequency in the interval 41-60 percent (Fig. 4). For more refined computations vertical correlation terms can be added, but for present purposes it is of interest that there is a sharp cutoff near 60 percent. The crowding of half of the values close to this limit denotes very substantial depletion of the available moisture. With such high values one can better understand the decrease of precipitation from the Pacific coast eastward, as well as the maintenance of deserts leeward of the mountain ranges. From the surface weather maps it appears probable that much of the water vapor condensing over the Wasatch mountains has not come over the coastal and intermediate mountain ranges, but that it has entered from the southwest avoiding high mountains. The same can be said for the lee side of the Wasatch. Precipitation at Grand Junction and beyond in the Rockies depends on moisture addition from the south, bypassing the main Wasatch range.

In Figure 5 we see a scatter diagram of the two efficiencies. It turns out that they are well correlated. It may be that, after examination of another and more moist season, one could use the simpler criterion of the abscissa for computation of a large sample. Note, however, that the basic technique remains construction of the energy tube. For addition of a line integral method, stations would have to be established in the lee of the mountains. The line integral method was tried with the synoptic stations on the large circle, but it was found unreliable with respect to the mountain precipitation and sometimes yielded impossible negative values. From Rasmussen et al. (1969) such calculations are more effective over plains and no doubt also over ocean areas.

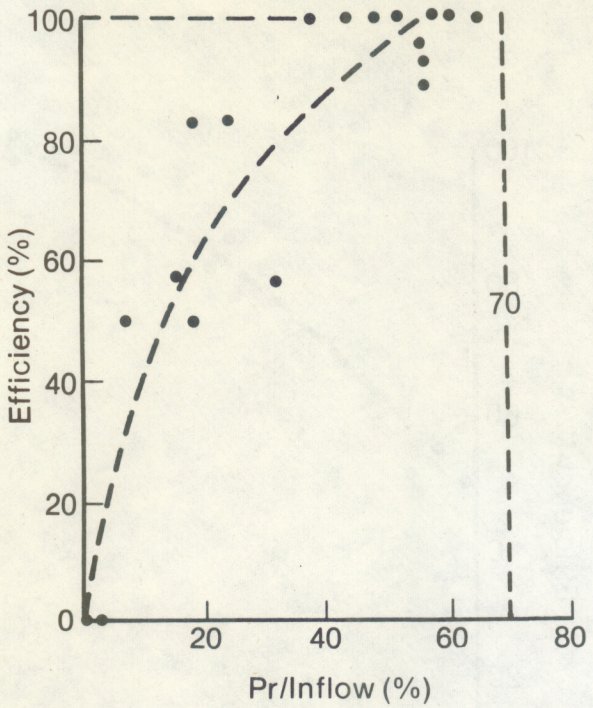

Figure 5.--Scatter diagram of efficiency from equation 7 vs. precipitate/inflow.

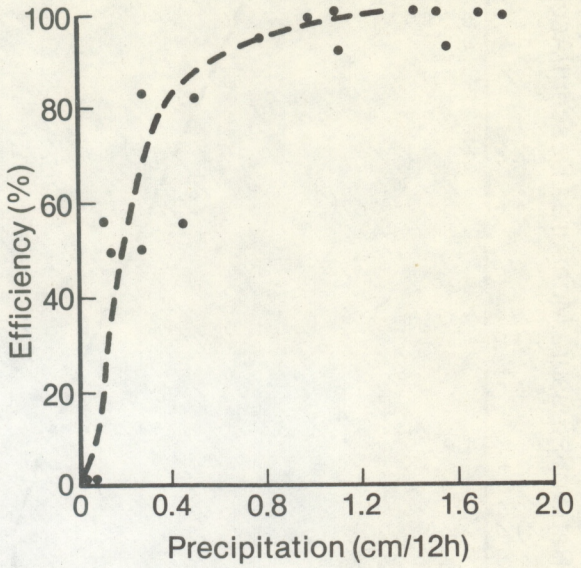

Figure 6.--Hypothetical distribution of efficiency against precipitation, assuming that all precipitation episodes had a duration of 12 hours.

We would have liked to go from Pr to P, but neither observed nor computed precipitation was available. At least one must know onset and termination times, hence duration. Possibly those can be extracted from the Utah climatological files. We had hourly data from a string of recording gages eastward from Beaver to the middle of the mountains; five gages were on the slope or on the top. For our cases that passed through the area, the number of hours with precipitation was tabulated for each station yielding 34 values. The range was 2-22 hours but there was a strong middle group of 10-14 hours with nearly half of the values. The mean was 10 hours and the median 11-12 hours. If we accept this duration for modeling purposes for all cases, a striking correlation between E and P results (Fig. 6). In spite of the imperfection it does become clear that high efficiency is related to high precipitation rate.

3.2 Ascent and Descent

In this section the ascent and descent of the energy tubes related to the variations in potential temperature shown in Figure 1 are discussed. At high efficiencies the ratio of pressure descent/ascent of the midpoint of the energy tubes is very small and approaches zero (Fig. 7). With increasing ratio the efficiency lowers and becomes about 75 percent when descent equals ascent. In three cases the descent carried below the ascent level, with efficiency decreasing to 30 percent. Of course, potential temperature still rises but by smaller amounts at high descent/ascent ratios when much of the condensate is re-evaporated.

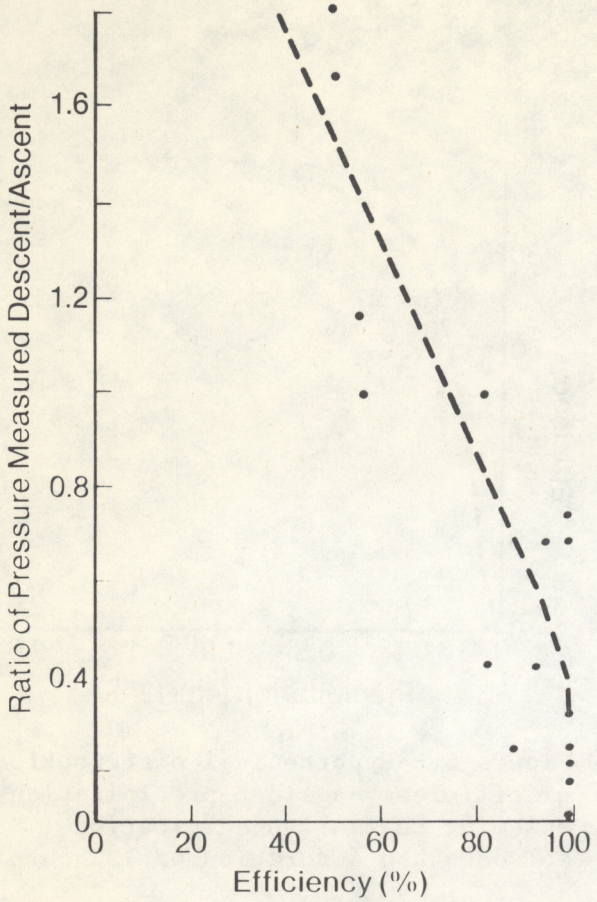

Figure 7.--Scatter diagram of efficiency vs. descent/ascent ratio of pressure change along the trajectories.

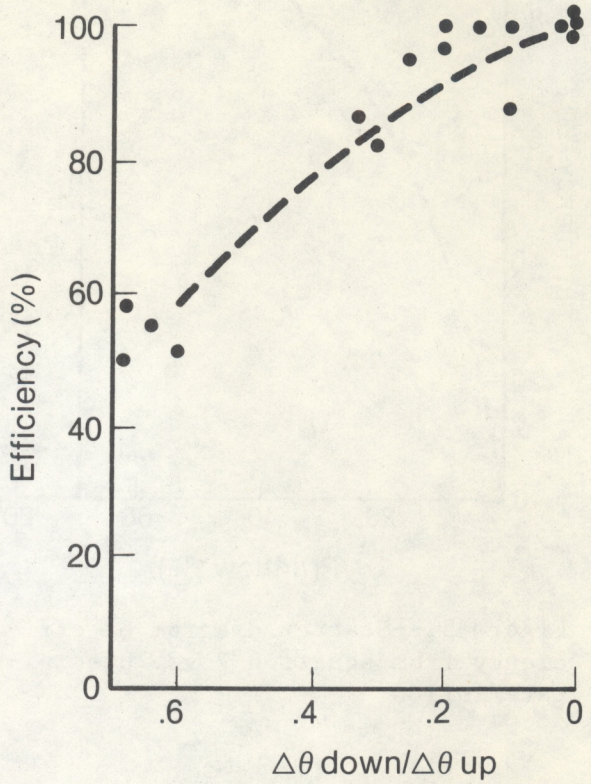

Figure 8.--Efficiency vs. (Δθ leeward/Δθ windward) of the mountain top.

Figure 8 offers the closest comparison with Figure 1; it shows E in terms of Δθ down/Δθ up. The actual paths are not readily comparable since total rate of gain in θ during ascent was too variable. Following is the frequency distribution of $(\Delta\theta)_{up}$ of the midpoint of the ascending column in intervals of 0.5°C, the closest value that could be read on the thermodynamic diagrams.

Degrees (°C)	n
1, 1.5	4
2, 2.5	3
3, 3.5	4
4, 4.5	0
5, 5.5	4

In most cases the midpoint experienced larger changes in θ than the top of the column where the flow often had become very flat. The expected distribution is largely in evidence in Figure 8. However, in a number of cases small net cooling rates up to 0.5 cal/g occurred, which may be ascribed to net radiation cooling during transit.

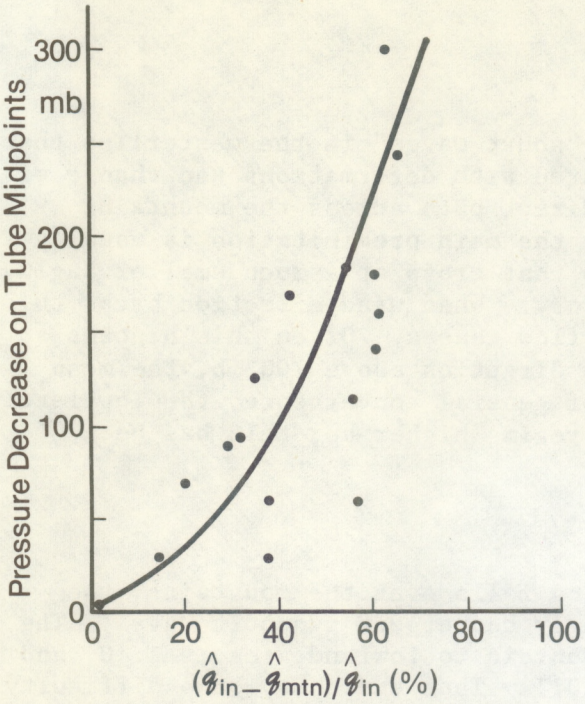

Figure 9.--Rise of the energy tubes in terms of pressure decrease of midpoint in terms of normalized condensate.

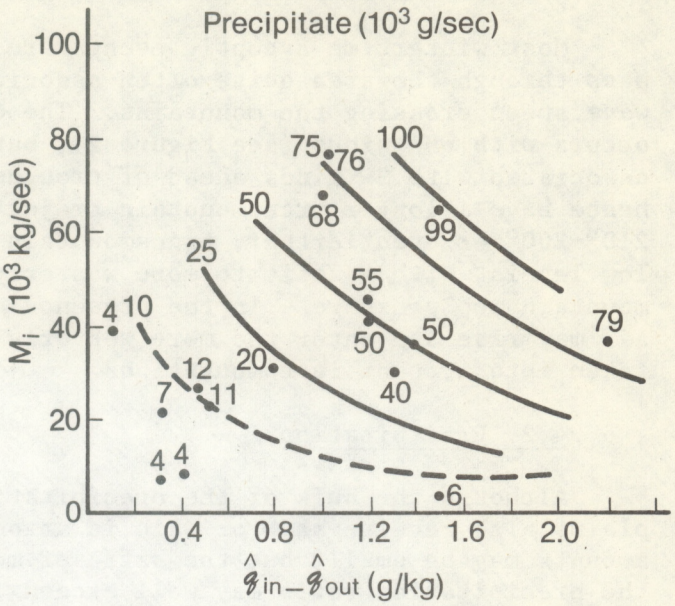

Figure 10.--Precipitate as a function of its two controls: mass inflow and specific humidity difference between inflow and outflow. Equivalent influence of both controls is seen.

Considering next the lifting of the whole tube as represented by the pressure decrease of the midpoint in terms of normalized condensate (Fig. 9), we find a good correlation, as might be expected. The regression equation is $y = 0.06\ x^2$, where y is the ordinate and x the abscissa. The condensate, like the precipitate, has an apparent limit near 60-65 percent, a high value. About 40 percent of the water vapor escapes without condensation even in the most efficient situations.

From Figure 9 one might conclude that the uplift alone is the essential mechanism in precipitation production. However $Pr = \hat{M}\ (\hat{q}_i - \hat{q}_o)$ is not dependent only on $\hat{q}_i - \hat{q}_o$ for which the mechanism is largely shown in Figure 9. In different cases M will vary and thereby also make a contribution. The question is solved in Figure 10, where precipitate is shown as a function of the two controlling parameters. If $\hat{q}_i - \hat{q}_o$ were the main control, there would

be a regression line at a small angle to the abscissa. If $\hat{M}$ dominated in shallow convergent altostratus, the regression line should lie at a small angle to the ordinate. From Figure 10 neither of the convenient solutions verifies. Rather do we find that both controls act as equally important mechanisms. Large mass flow at small $(\hat{q}_i - \hat{q}_o)$ and small mass flow at large $(\hat{q}_i - \hat{q}_o)$ can contribute equally to high efficiency.

4. The Synoptic Background

4.1 Waves in the Westerlies

Most wintertime synoptic events are "short waves" in the westerlies that pass through the area quite often associated with deformations and change of wave speed crossing the mountains. The direct path across the mountains occurs with WNW winds (see Figure 2), but the main precipitation is usually associated with SW winds ahead of troughs that cross at a much smaller angle, hence have a longer transmountain trajectory. When wind direction backs to 210°-200° or even farther, transmountain flow ceases. Often this happens at low levels, with a shift to more westerly direction above 700 mb, the mean mountain top pressure. In the presence of general convergence, the low-level air may rise and enter the more westerly regime higher up; this has been taken into account in computations.

4.2 Precipitation

Although the bulk of the precipitation falls over the mountains, the plains also receive snow or rain in strongly convergent synoptic waves. The amounts may be small, but the ratio of mountain to lowland area is 1:10, and the precipitation ratio may well exceed 10:1. Thus there may be a difficulty interpreting moisture brought in at ELY or DRA as precipitating (almost) exclusively over the mountains. Low-level precipitation has been followed with synoptic reports. Fortunately, the high lowland amounts occurred mainly north of the area considered, so that we believe only a small error has been made in neglecting precipitation over the southern Utah deserts. The stations along the immediate windward mountain side are included in our area measure. However, in other years there may also be cases with relatively heavy rain over the desert. Then winds over the mountains are likely to be S to SSW, and no computation is possible. In selecting cases one should be aware of the old principle: the stronger a general convergence zone, the more mountain effects recede in importance.

Problems from strong general convergence arose mainly when precipitation was reported in the lee (east side) of the Wasatch, especially at Grand Junction. Evidently, one cannot let transmountain trajectories descend under these circumstances, even though energy values may be identical, derived from low-level flow around the southern end of the mountains. In such cases our transmountain trajectory was held well above any precipitating cloud or overcast generated from below.

4.3 Classification

The particular synoptic synotic circumstances that prevailed during the analysis over the mountains have been classified in terms of flow and thermal advection:

Wind direction	n	Advection
SW	11	cold (7), mixed (4)
W	2	cold (1), zero (1)
NW	3	cold (3)
Circular	1	zero

The thermal advection refers to the layer 700-500 mb during the interval of the trajectory. Most trajectories crossed the mountains at the forward edge of the cooling trend which occurred with the approach and passage of waves in the westerlies.

4.4 Jet Streams

It turned out that the 300-mb flow field, representing the layer of maximum wind quite well in winter, had a marked influence. Jet stream cores of 100-150+ knots were present in all January and February cases, but they seasonally weakened in March. The precipitating trajectories were situated to the left or cyclonic side of the jet axes in 15 out of 18 cases; in 3 the shear changed from indifferent or weak anticyclonic to cyclonic at the end of the trajectory period. Most cases occurred with 300-mb cyclonic shear ranging from 20 to 40 knots per 100 miles. The amount of the shear appeared to have less importance than the sign. These are all instances of the vertical "indirect" circulation about polar jet streams first described at the University of Chicago (1947). This finding is in sharp contrast with summer precipitation when, with clouds mainly of the cumulonimbus type, anticyclonic high-tropospheric outflow predominates in numerous situations.

4.5 Thermal Stability

Although not strictly within the scope of this investigation, it was of interest to see whether systematic variations in thermal stability could be added to the rather decisive synoptic patterns mentioned. The first concern was with the temperature of the mountain sondes. It was found that along the mountain trajectory in an energy tube, the lapse rate following the tube always tended closely to the adiabatic with respect to water or ice, little different at the low temperatures. Thus, along the trajectories, neutral static stability prevailed. How were these faring in the given setting of vertical stabilities, however? The sondes, with one exception, were not convectively unstable, and therefore the trajectories could remain in approximate neutral equilibrium with their surroundings only if they moved from the starting point toward colder temperatures at upper levels. In an environment given by the initiating sonde the ascents would nearly all have been very cold and could not have attained the heights that were reached by them.

For a test it was assumed that the temperatures of all stations changed linearly and that therefore the temperature at top and bottom pressure of the mountain sonde, normally but not necessarily the middle time of the 12-h transmountain flow, could be determined. Isotherms for all cases were drawn for these two levels, of which Figure 11 shows the result for the two cases described later. We observe that there is no problem with the bottom in either case; in some others the bottom was actually warmer than the outskirts, suggesting a tendency to convection. The top of the mountain sondes happened to be coldest by 1°-2°C--which was not true in all cases. Such a small temperature difference is defensible, but it is seen that we certainly are not far from the highest cloud tops that could have occurred. In a number of cases the tropopause was a definite limiting barrier to vertical development.

The tube ascents were also classified in terms of deviation of lapse rate from the ice adiabatic as were all soundings on the circle and the special stations when relevant. The range of deviation was from -0.10°C/100 m to +0.10°C/100 m, where the negative sign stands for a steeper and the positive sign a more stable lapse rate than the ice adiabatic.

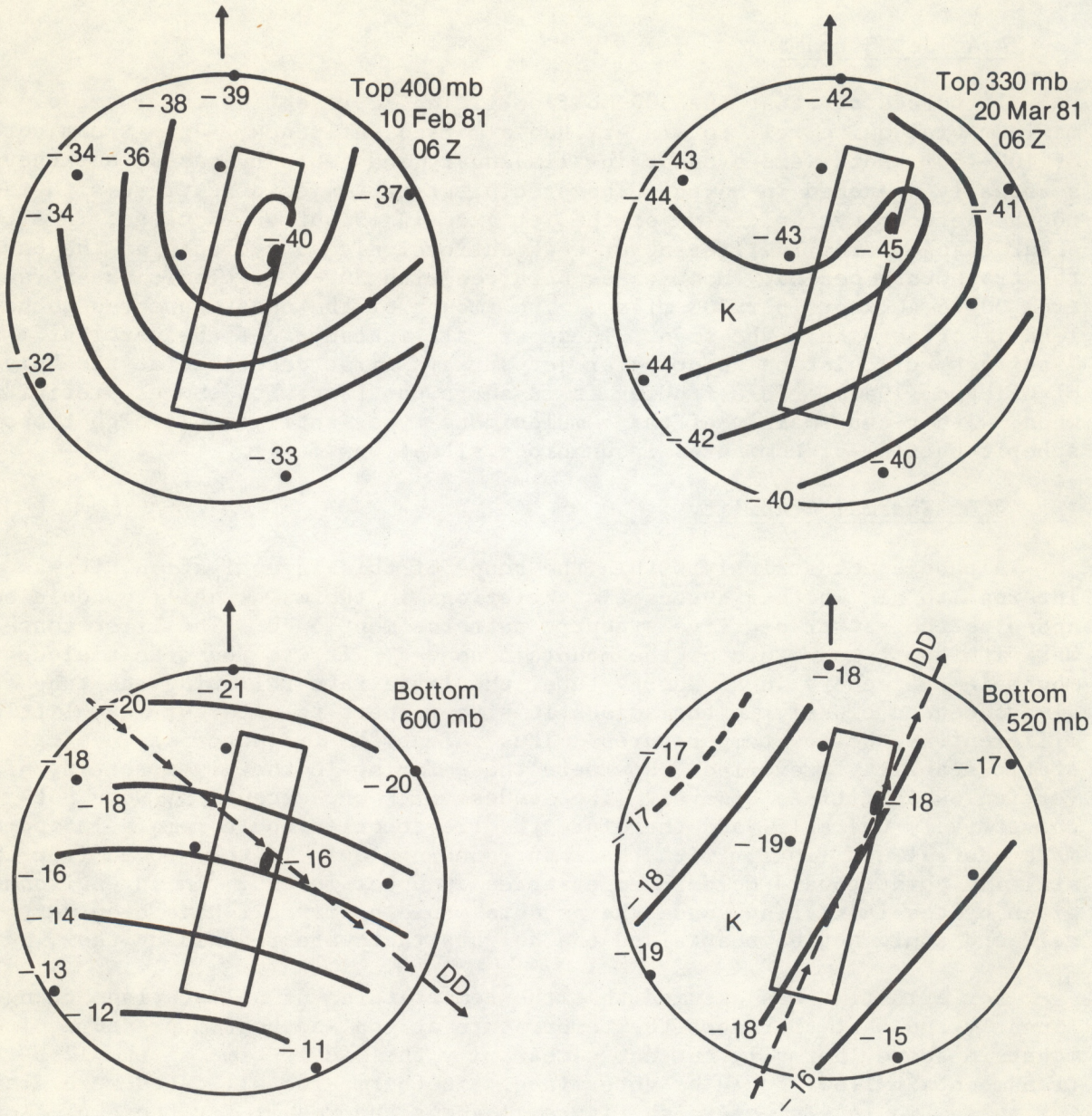

Figure 11.--Map of temperature at top and bottom of the mountain sonde at the time the trajectory reaches its highest elevation (location marked by heavy dot). (Left) 10 February 1981, 0600 GMT; (Right) 20 March 1981, 0600 GMT. Direction of trajectory is dashed line.

For each case the difference between the two sets of lapse rate variations was taken, i.e. the ascent lapse rate minus the mean of the surrounding lapse rates. Again, the range of the differences was from -0.10°C/100 m to +0.10°C/100 m; the negative sign now indicates instability of the tube ascent with respect to the environment. Only a small and not very consistent relation was found, not worth presenting. The considerations of Staley (1966) could not be followed since he confined his analysis to the nonsaturated case.

In conclusion, the energy tubes appeared to flourish best under the following three conditions:

(1) Low- and medium-level moisture supply.
(2) Presence of a baroclinic upper trough marked by cooling at all stations ahead of and even behind the axis. Most trajectories ran before the troughs.
(3) Presence of a jet stream core at 300 mb with cyclonic shear over the
mountain range with amounts from 20 to 40 knots/100 nmi, and, later in the season, presence of weaker cyclonic shear even without any intense jet stream center, with core speeds above 100 knots.

It follows that the synoptic circumstances very closely define the occasions when successful and highly efficient air trajectories across the mountains take place in winter synoptic systems.

5. Method of Computation Illustrated With Two Case Histories

Initially, one watches the synoptic charts, surface and upper air, as well as satellite photos for the arrival of upper troughs and fronts from northwest, west, and sometimes southwest. The numerical prognostic charts are consulted for speed of propagation, southward extension of troughs, and likely time of arrival in Utah. This, of course, is the identical routine followed by everyone else concerned. For illustration we choose first a northwest, then a southwest case.

5.1 The First Case

Probability of a precipitation event was heralded in the first case on 8 February; computations were started on 9 February, when a broad precipitation area moved eastward over Utah with southwest winds changing to west winds above 700 mb. Then a strong trough passed from the northwest, coupled with a polar outbreak from north at the surface; this outbreak brought the coldest temperatures of the winter for much of the whole mountain area. We will be concerned here with the first 12-hour period after trough passage from the Northwest, 00 GMT to 12 GMT on 10 Feb. 1981.

The width of the ring of stations is such that any trajectory over the mountains--head-on with northwest winds--will need 24 hours for 15-kn winds and 12 hours with 30-kn winds across the circle of Figure 2. From the sectional upper-air charts in Figures 12-13, 30 kn as an average fits quite well at 700 mb, so a trajectory of no more than 12 hours must be projected. At 500 mb the winds become stronger, and it must be assumed that the same properties are carried in this current for the concept of an "energy tube" to retain meaning. On some occasions, with still faster wind, 6-h sondes would be needed to find the energy in the outflow. These of course, do not exist. But

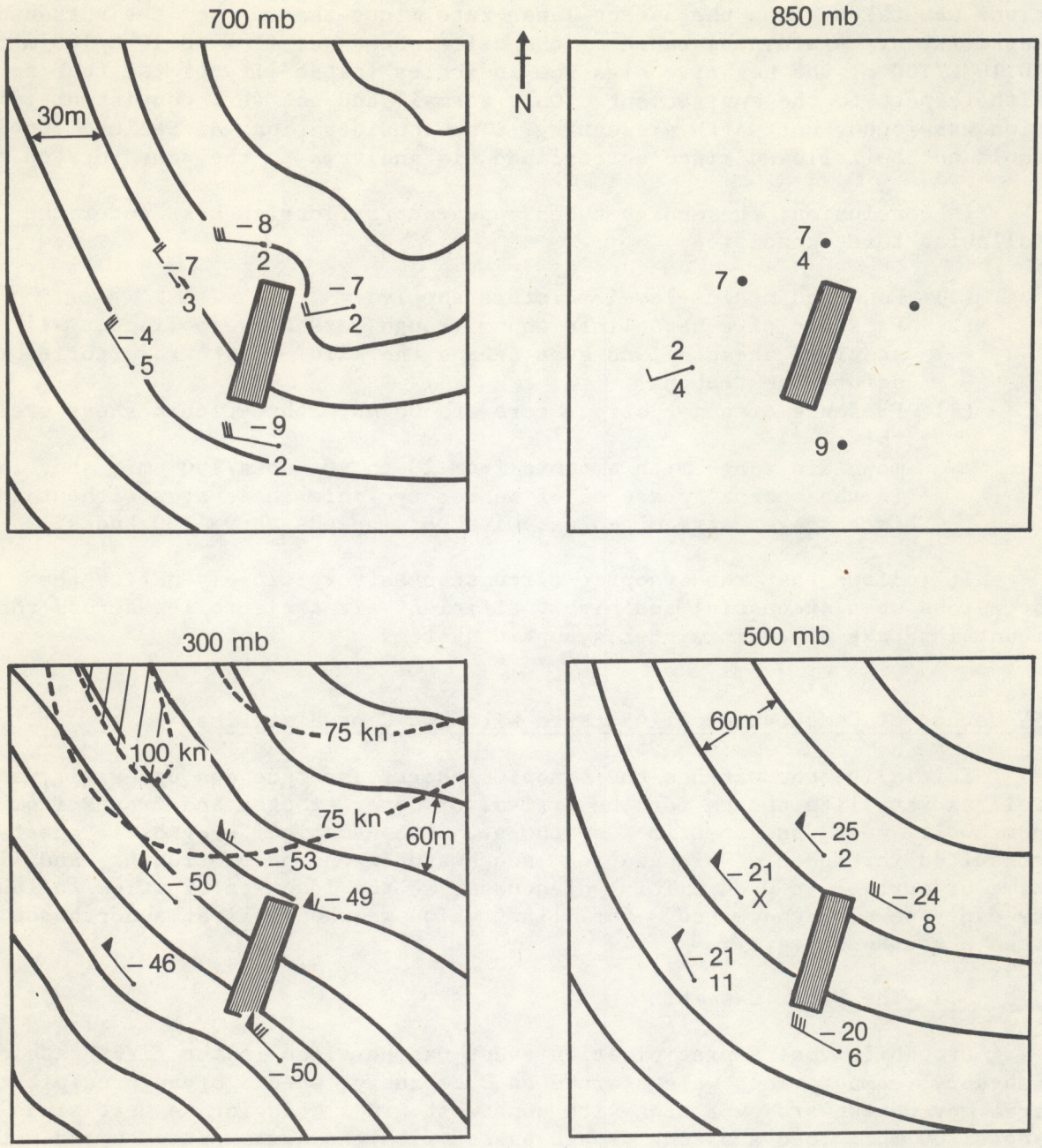

Figure 12.--Upper-air sectional charts for 10 Feb. 1981 (00 GMT) showing station temperature, dewpoint depression, winds, and location relative to the Wasatch mountain range. Solid lines are pressure surface contours with intervals as indicated; isotachs on 300-mb chart are denoted by dashed lines. See Figure 2 for station identification.

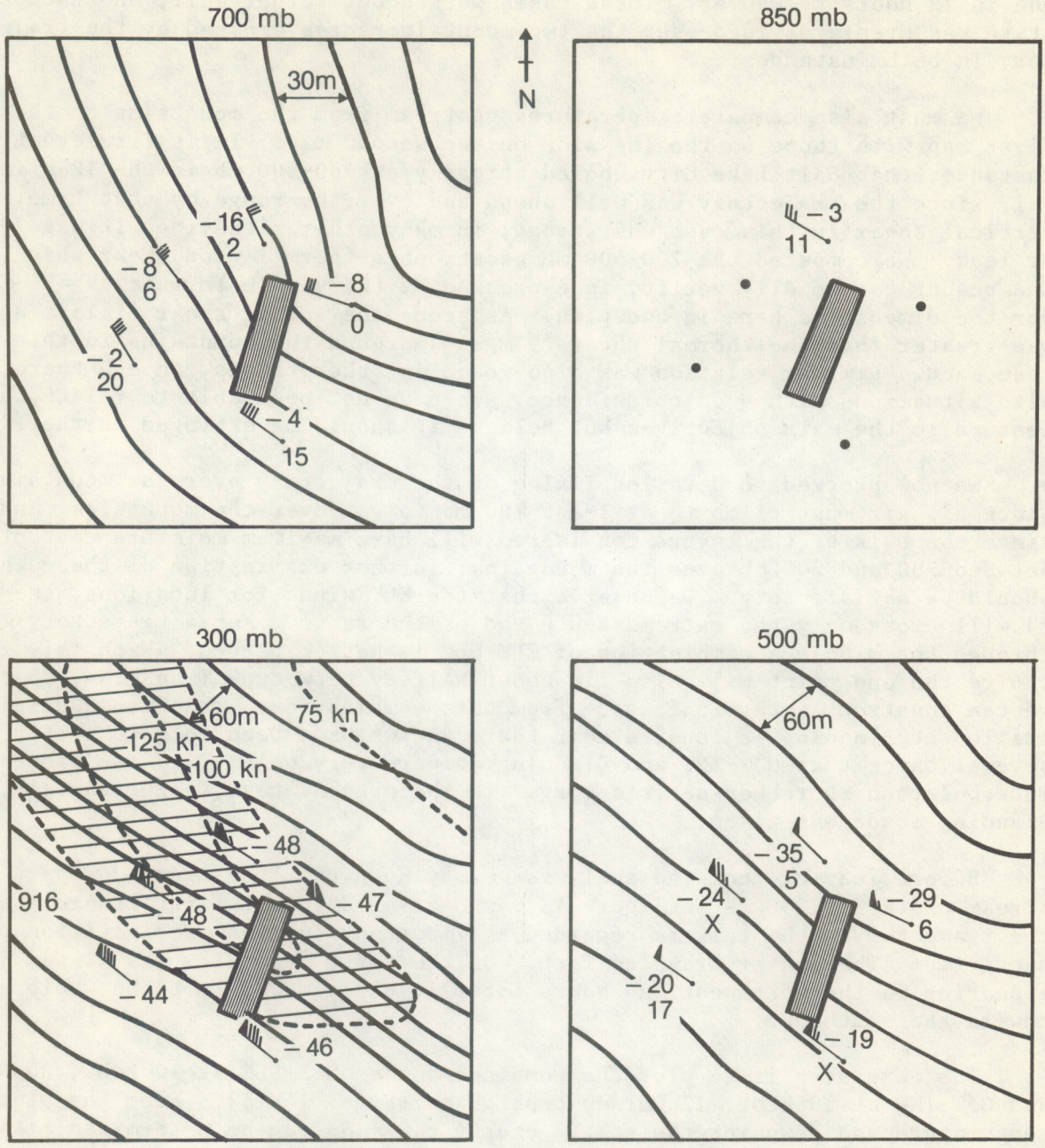

Figure 13.--Upper-air sectional charts for 12 GMT, 10 Feb. 1981 (see legend, Fig. 12).

we were able to lead one trajectory in 12 hours to Lander, Wyo., and another one in 12 hours to Denver. These cases worked out rather well, and the precipitate was evenly divided over the two mountain ranges crossed by the trajectory in both instances.

We must also compare temperatures upstream from the mountains on the first map with those on the lee side on the second map. It is irrelevant, for instance, that Salt Lake City cooled strongly at 700-500 mb in the 12-h interval, since the trajectory was well ahead and over the range by that time. The vertical shear in this case was strong; in many other situations it was 10 kn or less. We computed the 700-500 mb geostrophic thermal wind shear which, as the reader can readily verify, is expressed by the simple formula $dV = 2\,\frac{dT}{}$ for the dimensions here in question. As seen, the actual shear of 15 m s^{-1} was greater than the thermal shear (9 m s^{-1}) around the mountains in this case, and a similar relation was also found in other trials, though there were also situations with good coincidence. We have not been able to relate this feature to the main objectives but believe it should be explored further.

We now proceed to detailed fixing of the trajectory over the mountains. Since all air must climb to at least 700 mb to get over the mountains, and since the bulk of the layers considered will have maximum moisture content between 700 and 500 mb over the mountains, further examination of these charts should be satisfactory. We observe that the ELY wind (for locations, see Fig. 2) will cross only the extreme south end of the range. For a trajectory more through the middle a combination of ELY-SLC is better placed. With this choice the end point will also lie about halfway between GJT and INW, so that we can construct a terminal sonde from this combination. The Utah special station at Blanding is located near there and we have been able to verify in several cases that GJT-INW and Blanding compare very well; i.e. the linear interpolation is rather satisfactory. In the present case, unfortunately, no Blanding sonde was taken.

Before leaving the wind analysis we may note that the tremendous jet stream center at 300 mb in Figure 13 was bearing down with its forward nose on the trajectory path; this is regarded as important for the precipitation productivity. The center traveled fast. On the first map (Fig. 12) it was just appearing in the northwest; 24 hours later it had already left the whole area toward the southeast.

The next step is to plot the combined sondes ELY-SLC at 10 Feb., 00 GMT and GJT-INW at 10 Feb., 12 GMT on tephigrams (Figs. 14-15). From the plots of temperature and dewpoint the static energy $c_p\theta + Sq$ can be determined; it is shown in profile form in Figure 16. On the inflow side a tube with nearly constant energy is readily found at 65.6 cal g^{-1} with little variation between 800 and 560 mb. The pressure depth of 240 mb is rather a large one.

In general, following Rasmussen et al. (1969), a bandwidth of one cal g^{-1} or a width of 4 K in equivalent potential temperature θ_e has been found practical. Sometimes more than one tube can be located from a radiosonde ascent. The plot of Figure 16 is simple. On the outflow side we look for a layer with energy within one cal g^{-1}. It can here be located exactly at the inflow value but shrunk to 170 mb pressure depth.

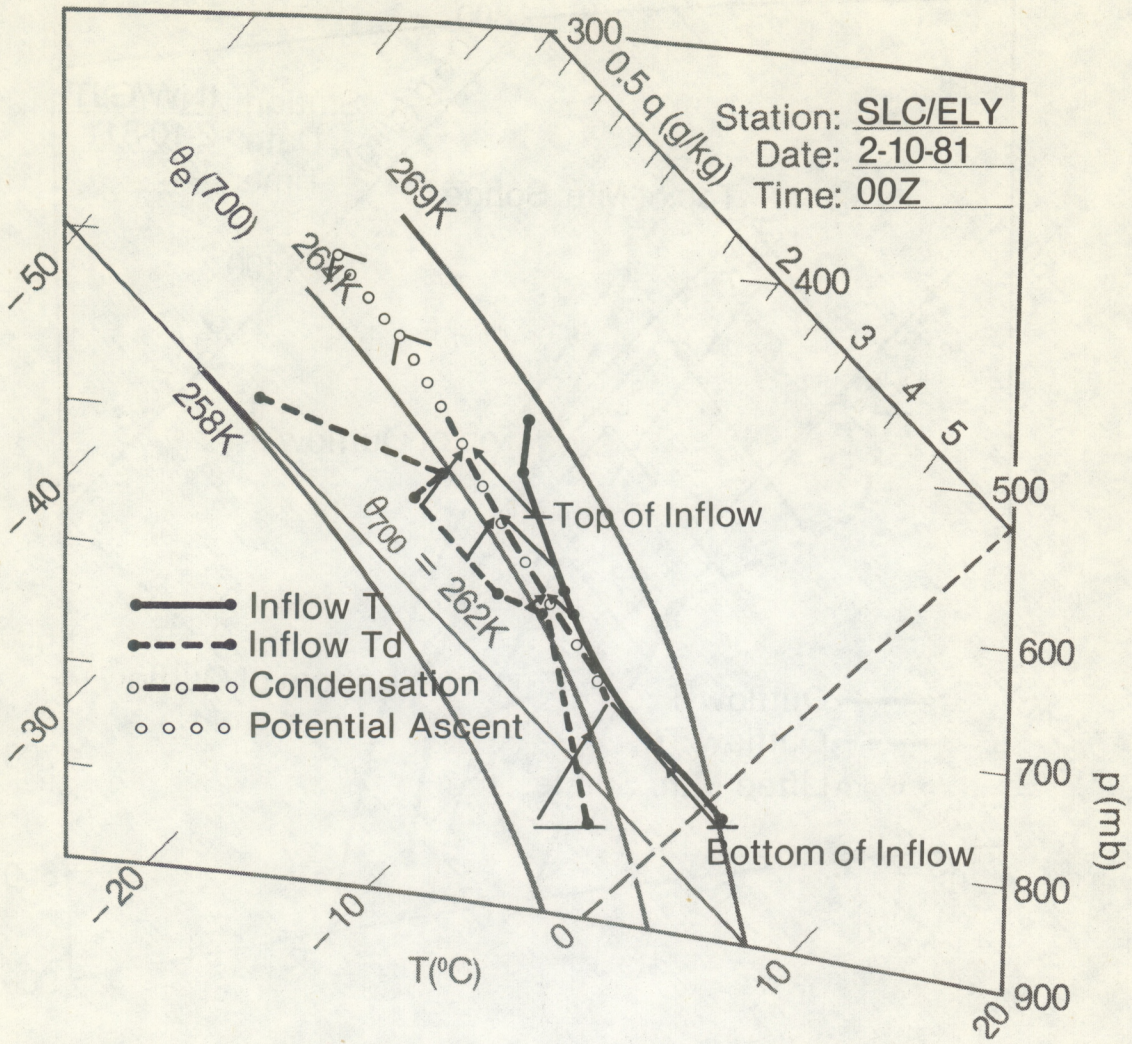

Figure 14.--Tephigram of the combined SLC/ELY inflow sonde at 00 GMT, 10 Feb. 1981, showing profiles of temperature, dewpoint, dry-adiabatic ascent to condensation (dash-dotted), and saturated ascent (open circles).

The inflow sonde (see Fig. 14) had a dry adiabatic layer from the surface (800 mb) to 700 mb with moderate moisture (relative humidity ranges from 60 to 75 percent). Above that, the lapse rate was slightly stable; relative humidity was high (75 to 90 percent) between 700 and 600 mb, and moderate (60 to 75 percent) above 600 mb. Because the lapse rate in the 800-700 mb layer was dry adiabatic, it is assumed that the layer became well mixed and was lifted to condensation with a mean specific humidity after mixing. All layers above 700 mb were lifted dry adiabatically to condensation. We now have a saturated sonde from 700 to 510 mb. However, the condensed particles are thought too small for precipitation to occur, and further lifting of the entire sonde was necessary for the droplets to grow. At pressures below 700 mb such lifting essentially occurs along an ice adiabat since temperatures go well below 0°C. For conversions from moist adiabat to ice adiabat, we start again with the first law where $c_p dT_1 + Ldq = 0$ and $c_p dT_2 + Sdq = 0$ at constant

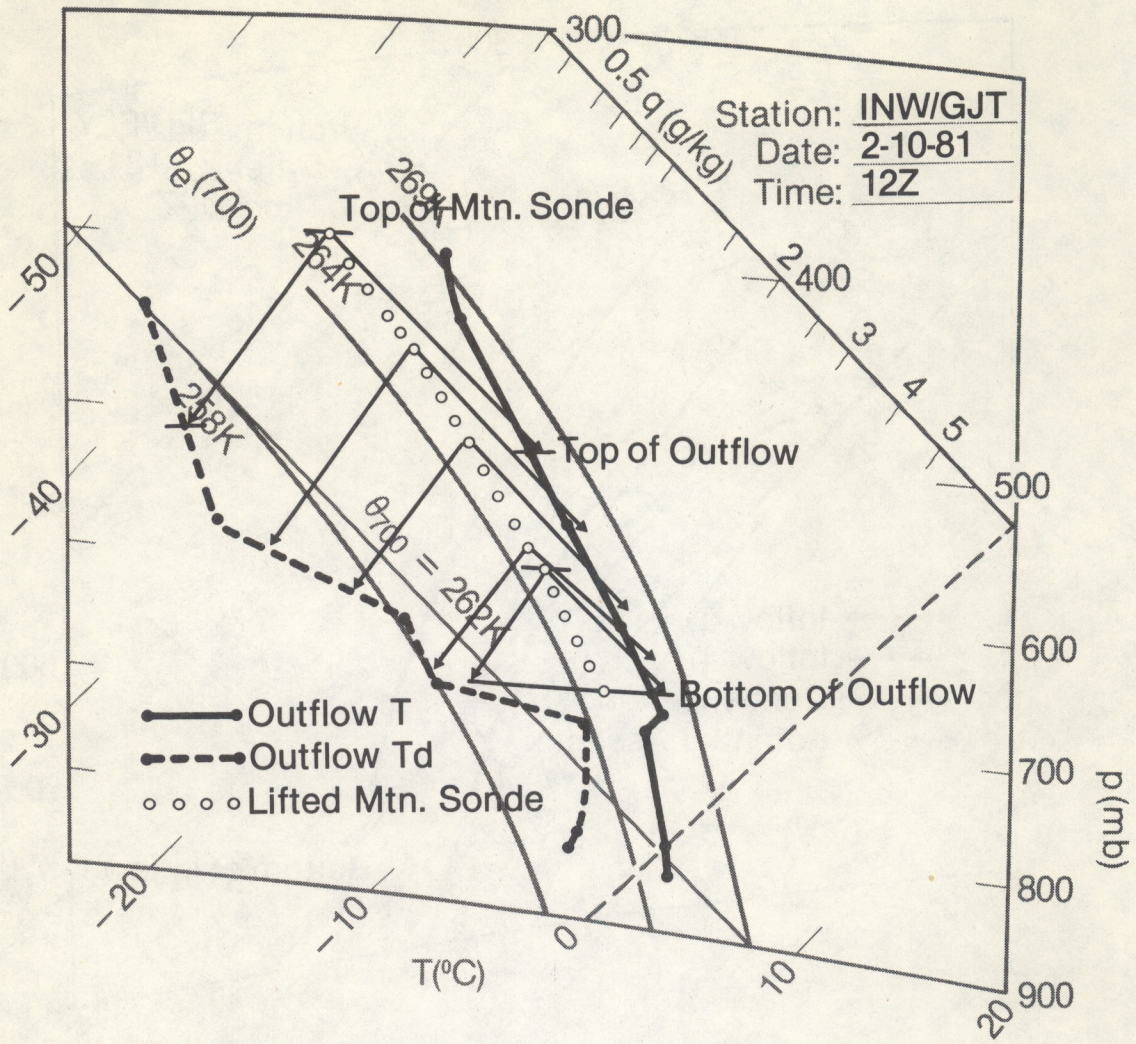

Figure 15.--Tephigram of combined INW/GJT outflow sonde at 12 GMT, 10 Feb. 1981, as in Figure 14 except that descending arrows are shown.

pressure for moist and ice adiabatic conditions, respectively. With dT_1 and dT_2 representing respective temperature changes of a parcel under moist and ice adiabatic conditions for a particular moisture content interval dq,

$$dT_1 = -(L/c_p)dq \quad \text{and} \quad dT_2 = -(S/c_p)dq,$$

so $dT_2 - dT_1 = (S - L)dq/c_p$, and we get

$$dT_2 - dT_1 = 0.3dq \qquad (8)$$

where dq is expressed in g/kg.

In some cases ascent carried no farther; then only a nonprecipitating cloud formed. But in most instances the ascent continued to lower pressures, forming precipitation-size particles.

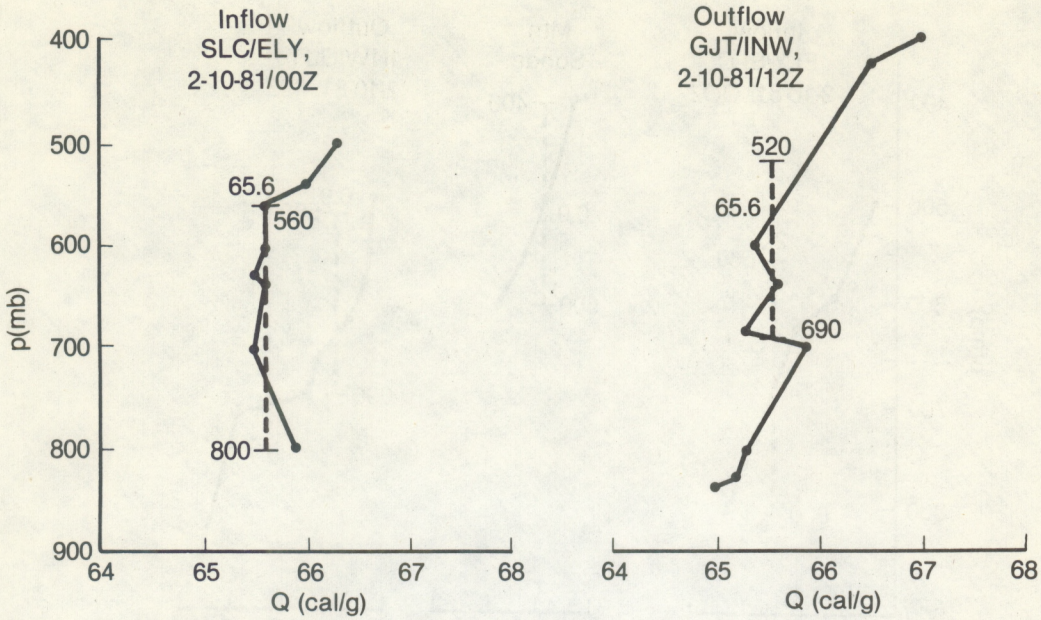

Figure 16.--Vertical profiles of total energy $c_p\theta + Sq = Q$ for the inflow layer (SLC/ELY at 00 GMT) and outflow layer (GJT/INW at 12 GMT) of 10 Feb. 1981. Selected constant energy tubes are dashed lines; pressure at top and bottom and mean energy value (cal g^{-1}) are indicated.

A top-of-ascent sonde can now be constructed (it will rarely be observed from radiosondes, though aircraft traverses could be usefully employed). To arrive at the highest point of ascent of the mountain sonde, it is necessary to examine the outflow sonde (Fig. 15) for the highest point to which a parcel in our energy tube can descend (in this case to 520 mb), by either dry or moist process. Similarly, the bottom of the outflow identifies the height to which the bottom of the mountain sonde descends. Having the same total energy for inflow and outflow sondes is not sufficient; the temperature and dewpoint profiles of the outflow must be such that a descent from the mountain sonde to the outflow is possible. In some cases such a descent was clearly not possible, even when total energies coincided.

The arrows in Figure 15 show how the mountain sonde fits the descent to the outflow layer. In this case, all layers descend dry adiabatically, and no evaporation occurs. We find the bottom of the mountain sonde near 600 mb and the top at 400 mb, easily identified in dry descent. The slight crossing of the descent arrows over the T-curve may be the radiation cooling.

The first calculation to be performed now is that of precipitation efficiency. Figure 17 gives the mean specific humidity for the inflow, mountain, and outflow layers, denoted by $\hat{q}_i$, $\hat{q}_{mtn}$, and $\hat{q}_o$ respectively. It is readily seen from (7) that $E = (2.3 - 0.9)/(2.3 - 0.9)$, for an efficiency of 100 percent. Herewith the principal objective of the analysis has been achieved.

As a second calculation we attempt to arrive at some estimate of precipitation on the plateau at 700 mb. The first step will be the determination of the precipitate. Thereafter the variable area (A) covered by the energy tube over the mountains and an arbitrary time factor will be included.

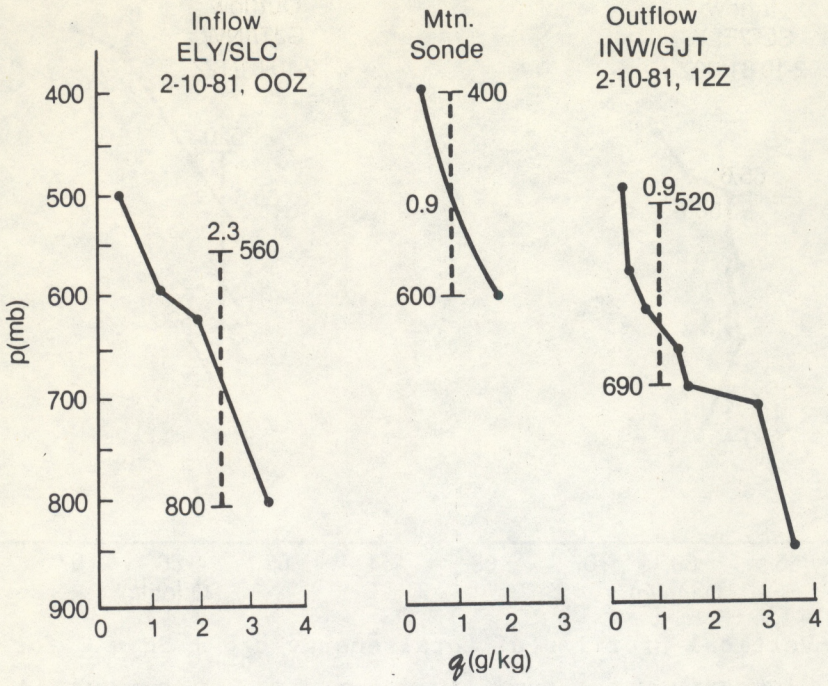

Figure 17.--Vertical profiles of specific humidity for the inflow layer, mountain sonde, and outflow layer of 10 Feb. 1981. Dashed vertical lines indicate mean specific humidity for selected energy tubes.

We start with determination of mass flow in the tube. Following the tube the equation of mass continuity states that

$$M = (V\Delta p/g)\delta n = \text{constant} \quad , \tag{9}$$

where M is the mass flow as before, V the total wind speed by definition of the "tube", $\Delta p/g$ its pressure thickness, and δn the cross-sectional width, here taken as 1 m for convenience in the inflow. From inflow and outflow hodographs of the wind (Fig. 18) the mean speed in the energy tube is determined as 30 kn for the inflow and 45 kn for the outflow. Inserting these speeds and the pressure differences in terms of kg m^{-2}, we find that $M_i = 36 \times 10^3$ kg s^{-1} and $M_o = 38 \times 10^3$ kg s^{-1}; i.e. they are virtually identical, and the energy tube preserves its cross section during the traverse. This is by no means always the case. Suppose, for instance, that M_o had come out as only half the value M_i. Then the cross section δn would have to be doubled to 2 m at the exit for the mass continuity requirement (9) to be satisfied. In other words, horizontal divergence would have occurred in the tube, requiring an increasing cross section with time. Such divergences, rarely convergence, are one main reason for the area A, over which the precipitation falls, to change. The other is the angle of attack of the flow against the mountains. With perpendicular flow we take the width as 100 km; with oblique flow it may increase to 150-200 km.

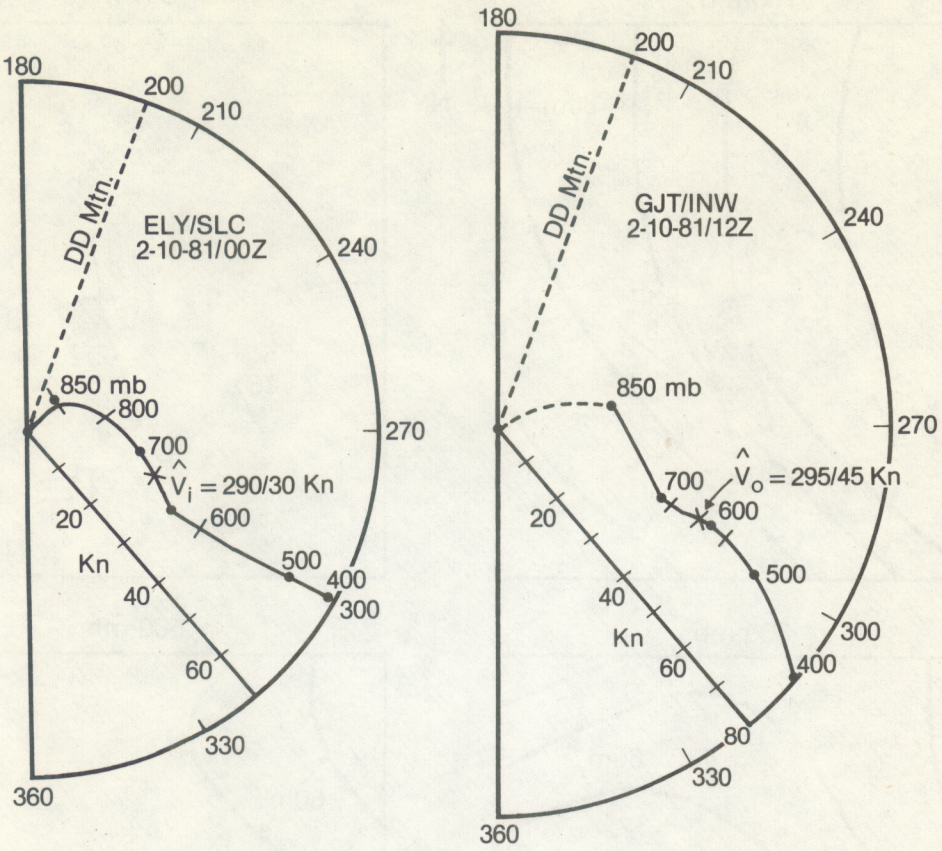

Figure 18.--Wind hodographs for the inflow layer (left) and outflow layer (right) of 10 Feb. 1981. Pressures are plotted along ascent/descent curves. Lower and upper limits of energy tube are marked by cross-bars; $\hat{V}$ denotes mean wind vector in tube. Outer scale identifies direction from which wind blows. Dashed line extending to 200° indicates the limit of wind direction required for cross-mountain traverses.

The precipitate $$Pr = M (\hat{q}_i - \hat{q}_o) \quad . \tag{10}$$

We have just determined M, and $\hat{q}_i$ and $\hat{q}_o$ are given in Figure 17. It turns out
that $Pr = 50 \times 10^3$ g s^{-1}.

Proceeding now to precipitation rate which is Pr/A, we find that the 1-m cross section remains unchanged because there is no horizontal convergence or divergence. Further, because the flow is largely but not entirely perpendicular to the mountains, a cross-mountain distance of 120 km applies. It follows that, if precipitation is expressed in g cm^{-2} per given time, then $P = 0.15$ g cm^{-2} h^{-1} or 1.8 g cm^{-2} 12 h^{-1}.

This event had the largest precipitation rate of all the cases studied, and it appears clear that all the mechanisms for an efficient system outlined in Section 4.5 are present. It is worthwhile to repeat that with its large precipitation rate this case also had the closest proximity of the jet stream maximum to the trajectory.

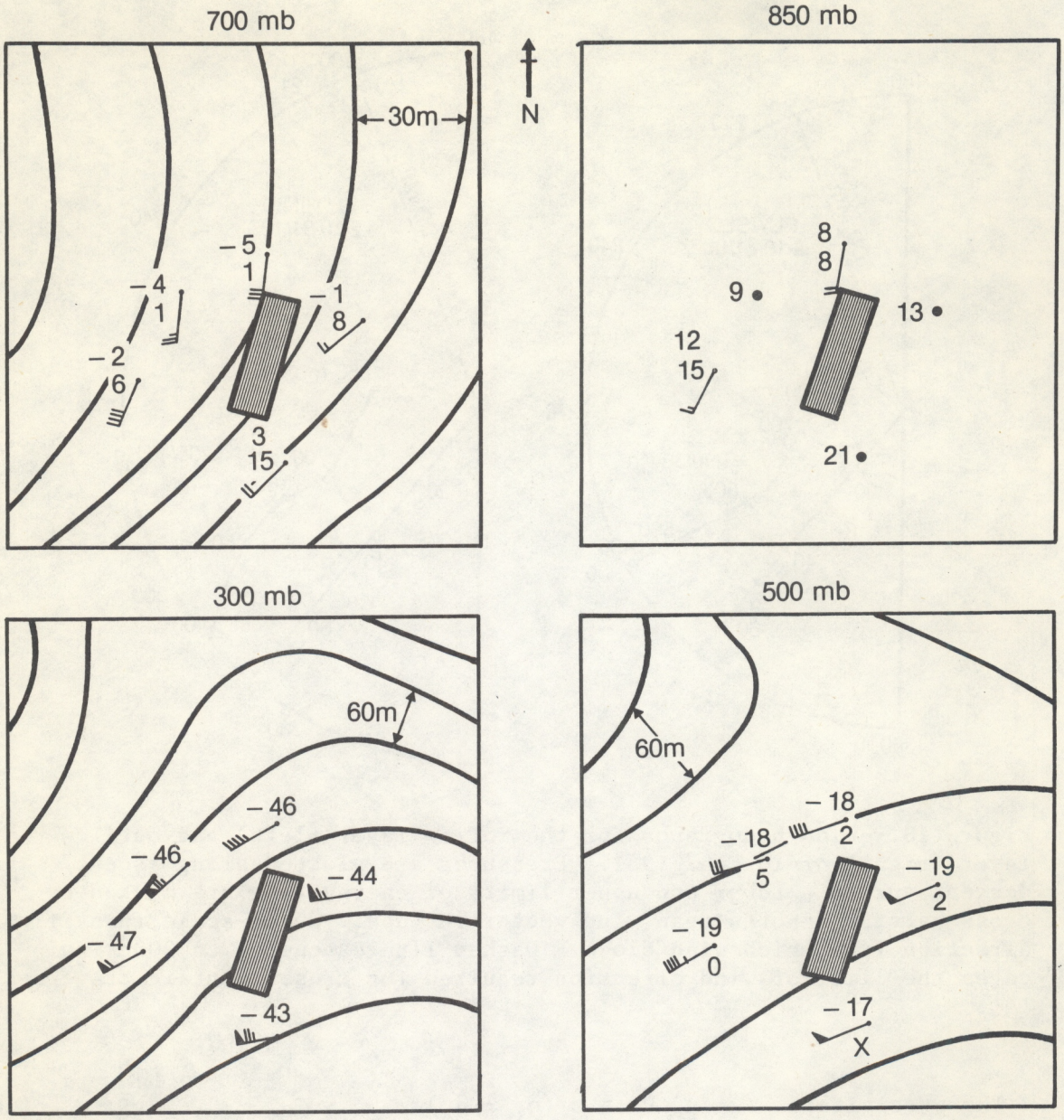

Figure 19.--Upper-air sectional charts for 20 March 1981, 00 GMT (notation as in Fig. 12).

5.2 The Second Case

The probability of a precipitation event for the second case was also announced by the approach of an upper trough. Precipitation began by 18 GMT on 19 March over the plateau west of the Wasatch Mountains, moving eastward to include the mountains by 00 GMT on the 20th. However, in this case the short-wave trough approached from the southwest, with south to southwest winds changing to southwest above 500 mb. Also, in this case the trajectory stayed in the southwest flow ahead of the trough.

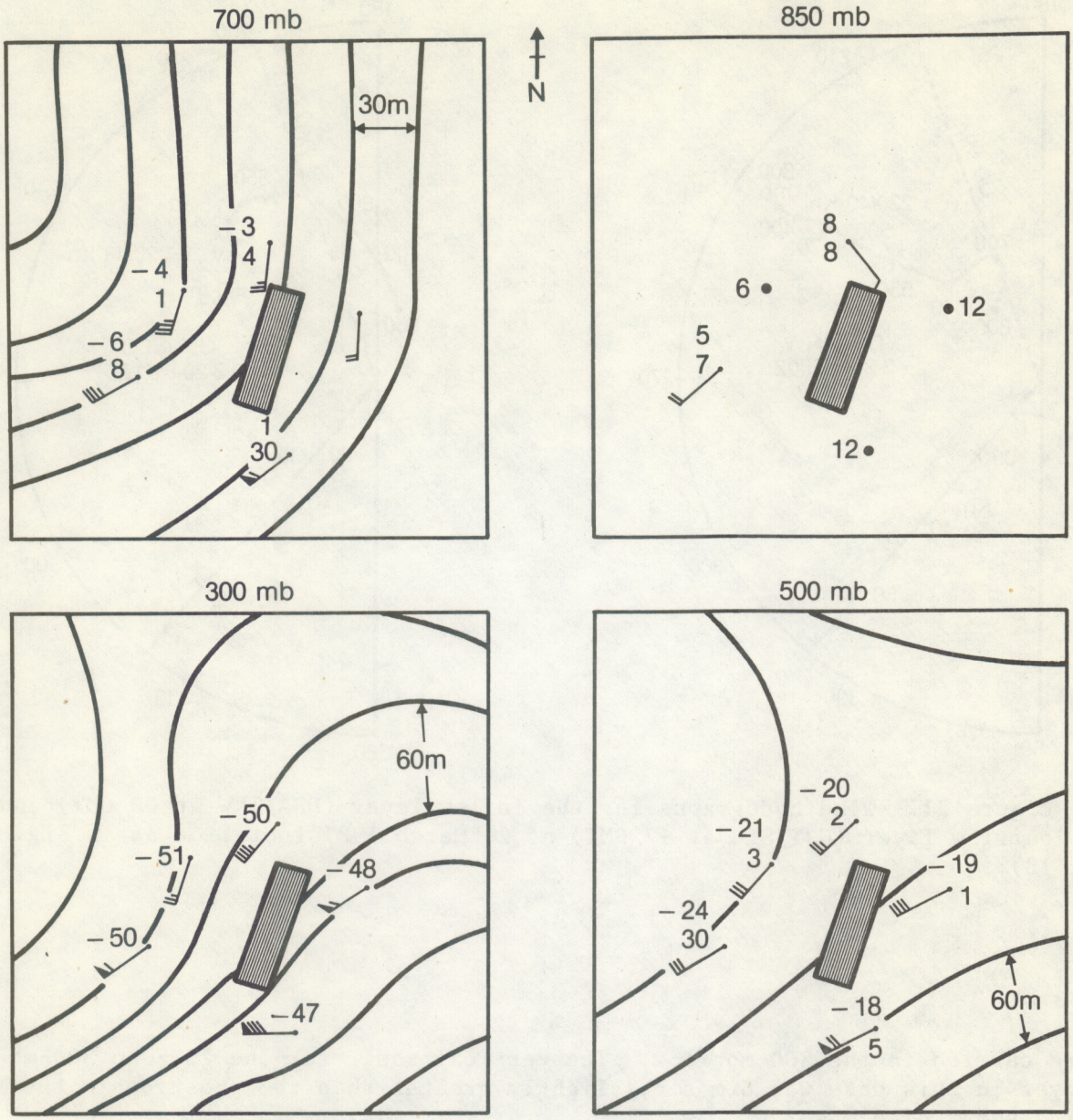

Figure 20.--Upper-air sectional charts for 20 March 1981, 12 GMT (notation as in Fig. 12).

As in the first case, there is the need to determine the length of time required for the trajectory. From the sectional upper-air charts in Figures 19 and 20, 30 knots as an average again fits well at 700 mb, so this trajectory also has a length of 12 hours. Care must be taken in cases involving large horizontal shear so that only winds near the approximate entry and exit points of the trajectory are considered. It is obvious, for example, that the wind at DRA at the end of the 12-h interval is unimportant, since the trajectory has long since crossed the range by then. Stronger winds are encountered at 500 mb, and it must again be assumed that the same properties

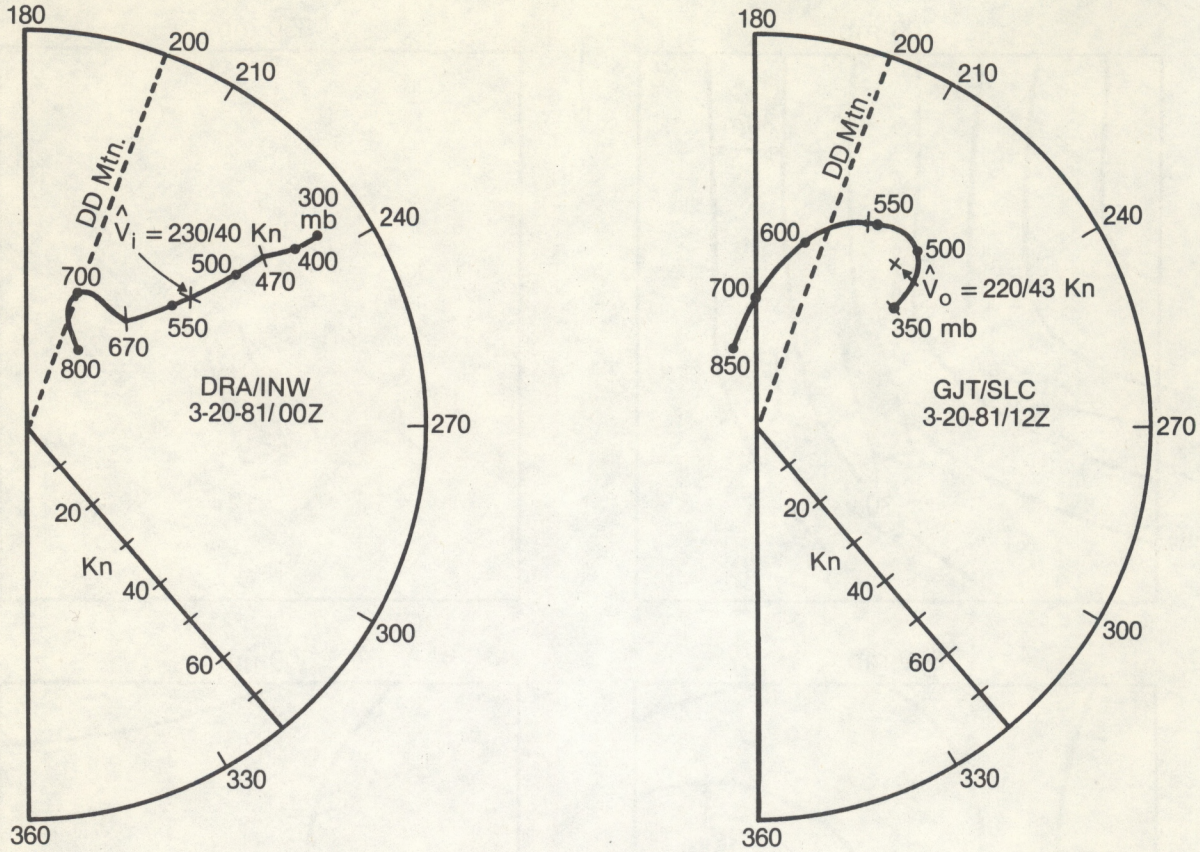

Figure 21.--Wind hodographs for the inflow layer (DRA/INW at 00 GMT) and outflow layer (GJT/SLC at 12 GMT) of 20 March 1981 (notation as in Fig. 18).

are carried in the 500-mb flow. The vertical shear for the 700- to 500-mb layer in this case was 8 m s^{-1}, slightly greater than the geostrophic thermal wind shear of 6 m s^{-1}.

Referring to the 700-mb and 500-mb charts on Figures 19 and 20, we see that with such a large southerly component to the flow, any air originating at DRA or ELY below the height of the mountains will not cross the range. To accomplish a trajectory over the mountains a combination of DRA and INW at higher levels must be selected, and even then the crossing angle would be small. This is especially apparent in the wind hodographs of Figure 21, which show that only inflow above 700 mb has an angle of direction greater than 200 degrees. The 200-degree line (dashed) shows the limit of flow angle required for cross-mountain traverses. Any wind with an angle of direction less than 200 degrees is not expected to cross the range unless it rises into the middle troposphere. The end point, therefore, will lie between SLC and GJT, so that the best terminal sonde would be constructed from this combination. The 300-mb sectional charts show that the strongest winds remained to the right of the trajectory, though this is much more apparent at 12 GMT than at 00 GMT; the cyclonic shear strengthened during the time interval.

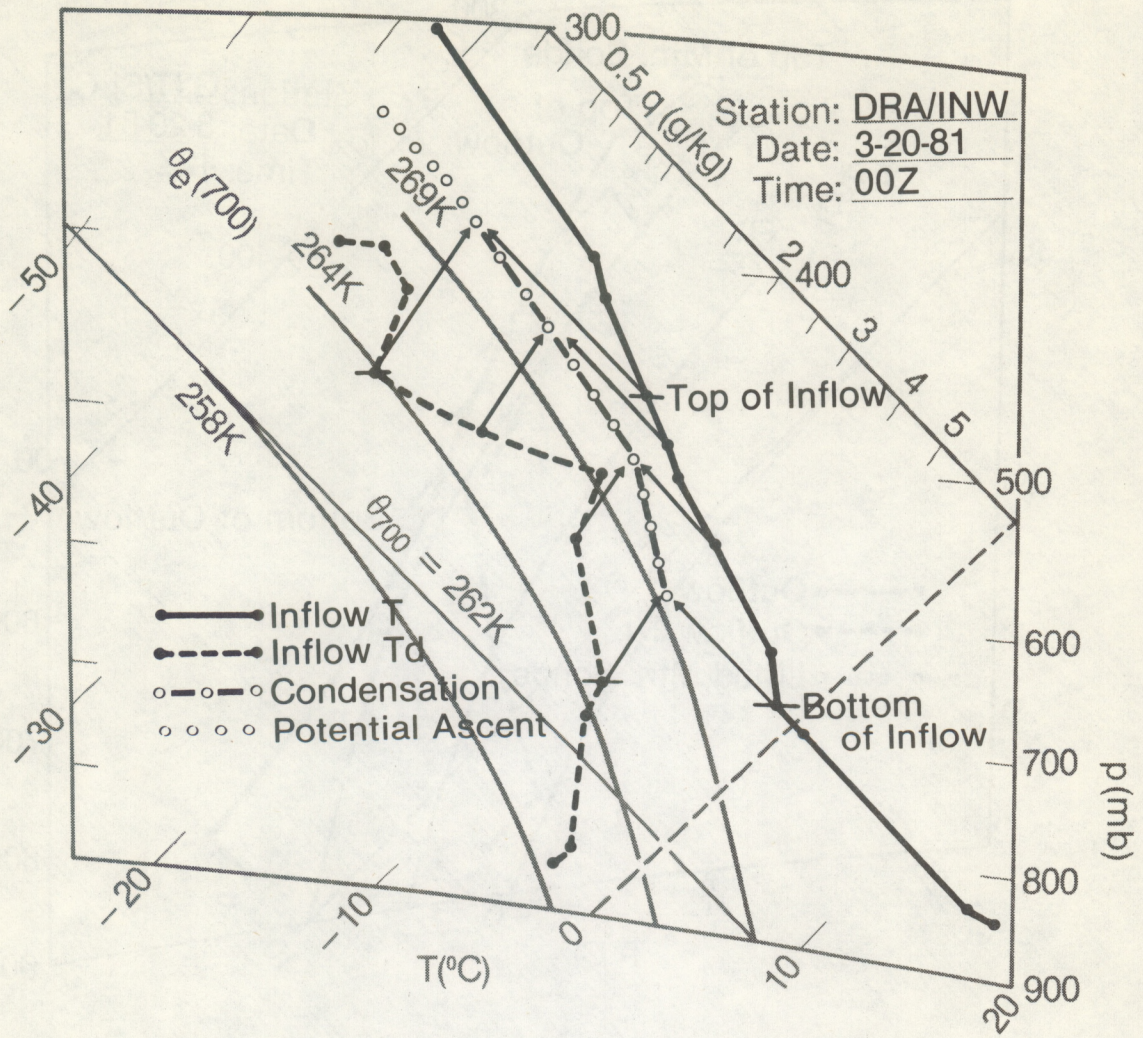

Figure 22.--Tephigram of the combined DRA/INW inflow sonde at 00 GMT, 20 March 1981 (notation as in Fig. 14).

Sondes are plotted this time for DRA-INW at 20 March at 00 GMT and for GJT-SLC at 12 GMT (Figs. 22 and 23). An inflow tube with wind at 240 degrees from 670 mb up (Fig. 21) and a mean energy of 68.1 cal g^{-1} is found between 670 and 470 mb (Fig. 24), for a pressure depth of 200 mb. The energy profile of the outflow had no distinct layer with constant energy; values increased steadily upward. For a mean energy of 68.0 cal g^{-1}, a tube comprising a full bandwidth of one cal g^{-1} is found between 555 and 350 mb, with 555 mb the lowest level at which air could have crossed the mountain (Fig. 21).

The inflow sonde of Figure 22 had a deep dry adiabatic layer from the surface (850 mb) to 670 mb with low moisture (relative humidity ranging from 20 to 55 percent). The profile had a lapse rate close to neutral above 670 mb, becoming slightly stable above 400 mb. Relative humidity was moderate, about 50 to 70 percent. The entire inflow layer between 670 and 470 mb is lifted dry adiabatically to condensation, the lifting denoted by arrows and the condensation by dashes and circles. Further lifting must take place for

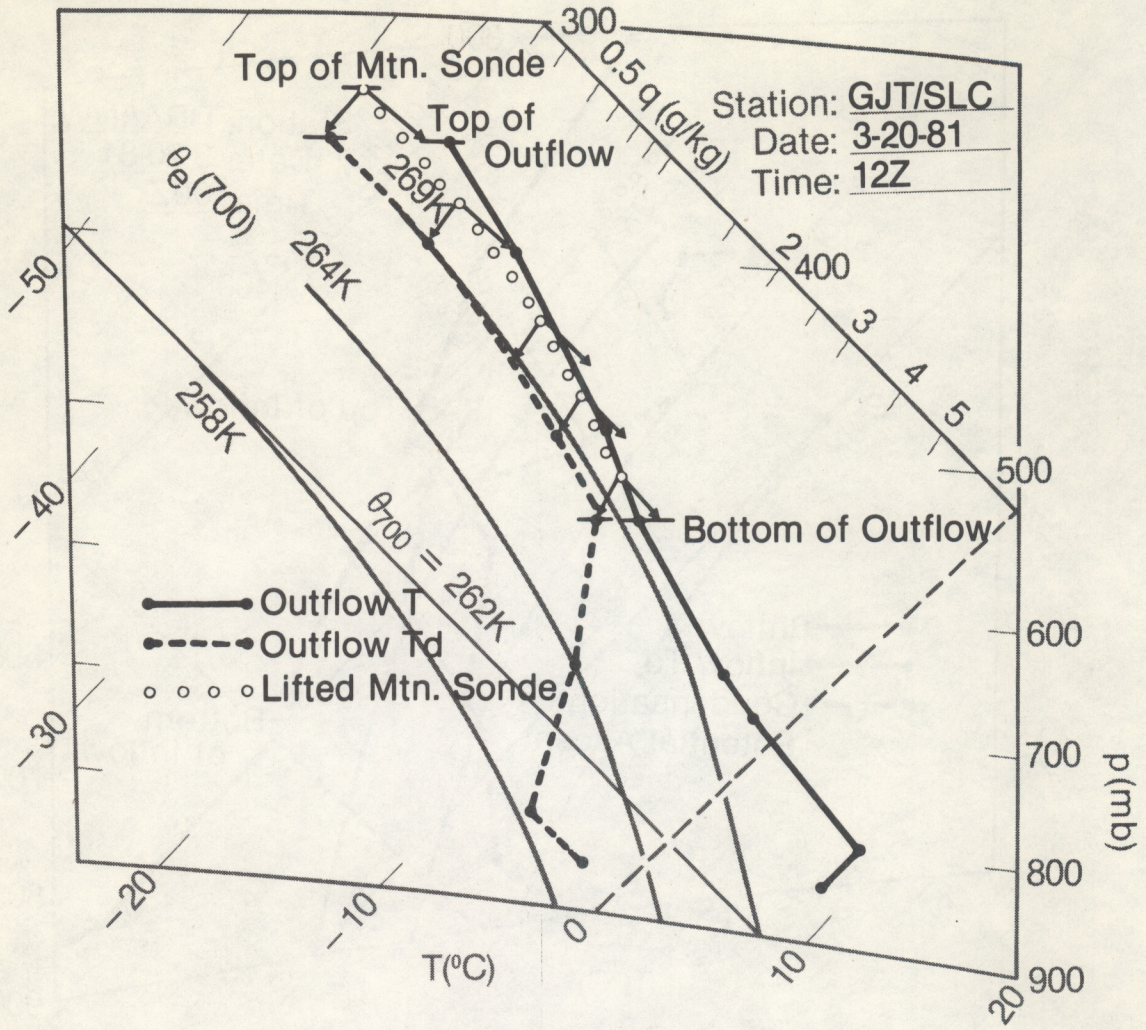

Figure 23.--Tephigram for combined GJT/SLC outflow sonde at 12 GMT, 20 March 1981, as in Figure 22, except that descending arrows are shown.

precipitation-size particles to develop and, as in the first case, the lifting takes place close to an ice adiabat, with the relation between moist and ice adiabatic processes given by (8).

The top-of-ascent sonde is constructed from the SLC-GJT combined outflow sonde for 12 hours later (Fig. 23). This sonde had an inversion below 800 mb, then a dry adiabatic layer to 690 mb. Moisture was low in these layers. The lapse rate above 690 mb gradually stabilized while relative humidity increased above 700 mb, going from 55 percent to 85 percent at 555 mb, the lowest point of descent from the mountain sonde. From there, relative humidity decreased to about 60 percent at 350 mb, the highest point of descent. As apparent from Figure 23, the top of the mountain sonde descends dry adiabatically to 350 mb with correct moisture but temperature 1°C low, which is in the expected range of accuracy. Lower down, the dry descents to the bottom of the mountain sonde all fall on the warm side of the terminal temperature curve. A certain amount of evaporation must have taken place, since radiation cooling alone is insufficient to account for the difference.

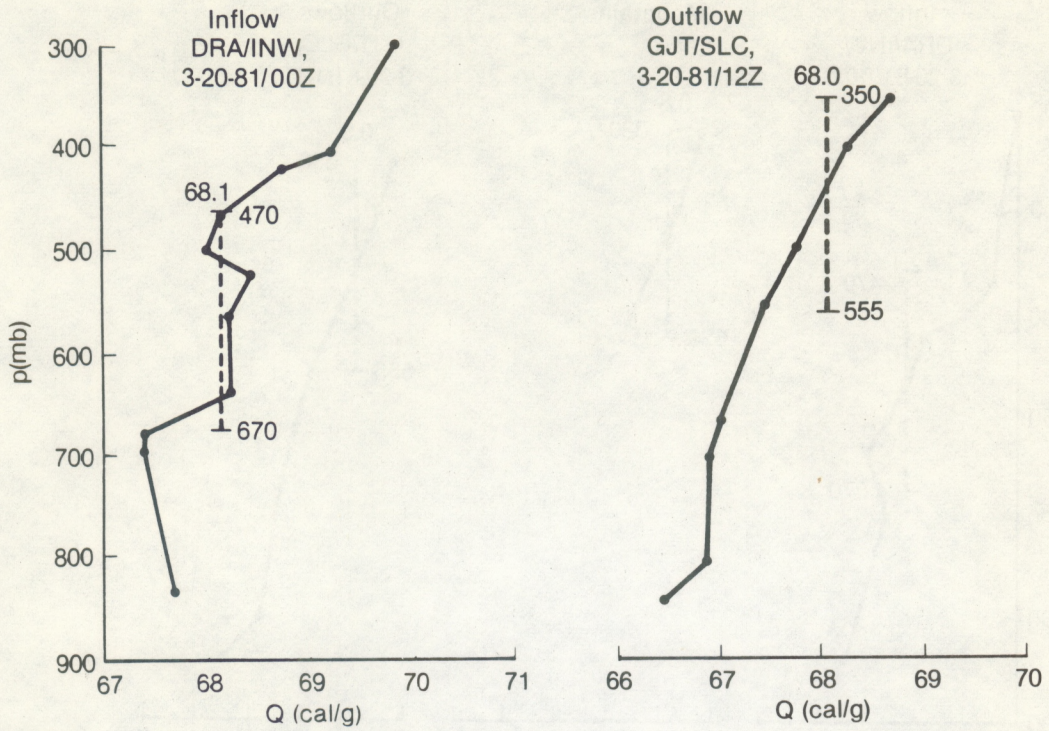

Figure 24.--Vertical profiles of total energy $c_p\theta + Sq = Q$ for the inflow layer and outflow layer of 20 March 1981 (notation as in Fig. 16).

The above also can be seen from the mean moisture curves (Fig. 25) where $\hat{q}_{mtn} = 0.8$ g kg^{-1} at the top and $\hat{q}_o = 0.9$ g kg^{-1} in the outflow. Given $\hat{q}_i = 2.1$ g kg^{-1} the efficiency from (7) is 92 percent, still a very high value.

For an estimate of precipitation we start again with a determination of mass flow. From inflow and outflow wind hodographs (Fig. 21) the mean wind speed in the energy tube is 40 kn for the inflow and 43 kn for the outflow. Inserting these wind speeds and the pressure differences in terms of kg m^{-2} into (9), we find that $M_i = 40 \times 10^3$ kg s^{-1} and $M_o = 43 \times 10^3$ kg s^{-1}. Again, the flow is essentially two-dimensional.

Using (10), we find that the precipitate Pr = 48×10^3 g s^{-1}, where $\hat{q}_i$ and $\hat{q}_o$ are as given in Figure 24, $M \sim M_i$ = constant.

However, for the precipitation rate Pr/A, the 1-m cross section remains unchanged as just found, but the angle between the flow and the range is very small (only about 25 degrees). Therefore the cross-mountain distance is larger, 200 km for this case. If precipitation is expressed in g cm^{-2} per given time, the P = 0.09 g cm^{-2} h^{-1} or 1.08 g cm^{-2} 12 h^{-1}.

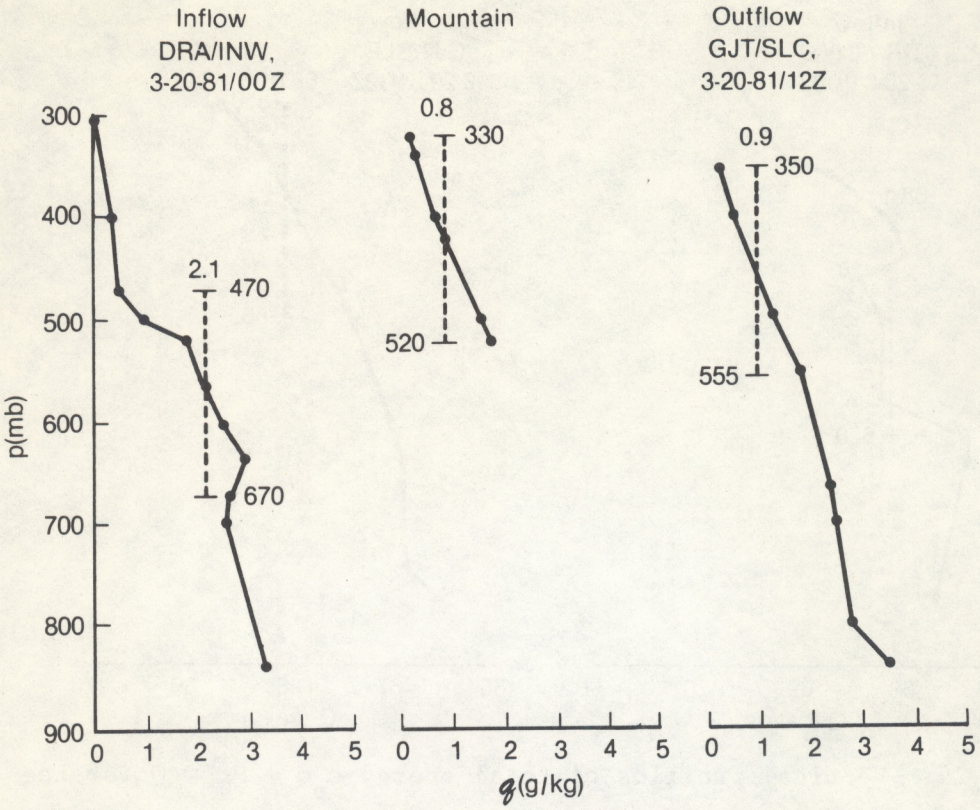

Figure 25.--Vertical profiles of specific humidity for the inflow layer, mountain sonde, and outflow layer of 20 March 1918 (notation as in Fig. 17).

In this case, not all the features described in Section 4.5 as most favorable for precipitation efficiency are easily identifiable. The presence of an upper trough is quite apparent, but only moderate moisture is found on the inflow. From the 500-mb sectional chart of Figure 19, with saturated air at DRA and very dry air at INW, it appears that most of the moisture entering the area of interest does not cross the range. Also, the cyclonic shear is not very large, especially at the start of the period, where it is hardly identifiable. Nevertheless, the efficiency remains large, primarily because the trajectory after ascent goes nearly straight across; i.e., it does not descend to levels where a large amount of moisture in gaseous form would flow out after evaporating.

6. Conclusion

The examples have shown that it is possible to arrive at a reasonable description of the physical processes and its consequences in terms of precipitate over the Wasatch mountains by employing the LaGrangian technique of following column trajectories, given the weak observational background. In this first effort the principal decisions were qualitative, mainly the selection of constant energy tube and of the technique of constructing the mountain sonde. Possibly more quantitative techniques may be developed for treating a

large sample of historical data. For future programs it is recommended that two additional stations be established at operational airfields in the immediate lee of the mountains; further, it would be most advantageous to make actual observations of the columns at the top of the mountains with ground-based or aircraft-based equipment.

7. Acknowledgments

B. Miller, Utah State University, kindly supplied copies of the rawinsonde observations taken by the three Utah-operated stations, as well as hourly precipitation data from the special snow gages in the middle of the Wasatch range near and east of Beaver. Mr. L. Snellmann, National Weather Service, is due thanks for the precipitation records of the NWS stations. The authors further wish to acknowledge the consistent support of Merlin Williams, NOAA/ERL, for this project.

8. References

Hill, G.E., 1977: Evaluation of southern and central Utah cloud seeding program. Report A1, Utah Water Research Lab., Utah State University, Logan, Utah 84322.

Rasmussen, J. L., Furman, R. W., Riehl, H., 1969: Moisture analysis of an extratropical cyclone. Arch. Met. Geoph. Biokl. Ser. A 18:275-298.

Staley, D. O., 1966: The lapse rate of temperature following an air parcel. Quart. J. Royal Meteorol. Soc. 92:147-150.

University of Chicago (Staff Members, Dept. of Meteor.), 1947: On the general circulation of the atmosphere in middle latitudes. Bull. Amer. Meteorol. Soc. 28:255-280.